Looking for the interactions between omeprazole and amoxicillin in a disordered phase. An experimental and theoretical study

Marcos G. Russo, Matias I. Sancho, Lorena M.A. Silva, Hector A. Baldoni, Tiago Venancio, Javier Ellena, Griselda E. Narda

PII: S1386-1425(15)30310-3
DOI: doi: 10.1016/j.saa.2015.11.021
Reference: SAA 14163

To appear in:

Received date: 5 February 2015
Revised date: 8 October 2015
Accepted date: 20 November 2015

Please cite this article as: Marcos G. Russo, Matias I. Sancho, Lorena M.A. Silva, Hector A. Baldoni, Tiago Venancio, Javier Ellena, Griselda E. Narda, Looking for the interactions between omeprazole and amoxicillin in a disordered phase. An experimental and theoretical study, (2015), doi: 10.1016/j.saa.2015.11.021

Looking for the interactions between omeprazole and amoxicillin in a disordered phase. An experimental and theoretical study

Marcos G. Russo[a], Matias I. Sancho[b], Lorena M. A. Silva[c], Hector A. Baldoni[d], Tiago Venancio[c], Javier Ellena[e], Griselda E. Narda[a*]

[a]Inorganic Chemistry - INTEQUI. National University of San Luis. Chacabuco and Pedernera - 5700. San Luis. Argentina

[b]Physical Chemical Laboratory, National University of San Luis. Chacabuco and Pedernera - 5700. San Luis. Argentina

[c]Chemistry Department. Federal University of São Carlos. PO Box 676. 13565- 905. São Carlos. Brazil

[d]Institute of Applied Mathematics San Luis (IMASL - CONICET). National University of San Luis. Chacabuco and Pedernera – 5700. San Luis. Argentina

[e]Physics Institute of São Carlos, University of São Paulo, CP 369, 13560-970 São Carlos, SP, Brazil.

[*] E-mail: gnarda@unsl.edu.ar

Abstract

In this paper, co-grinding mixtures of omeprazole-amoxicillin trihydrate (CGM samples) and omeprazole-anhydrous amoxicillin (CGMa samples) at 3:7, 1:1 and 7:3 molar ratios, respectively, were studied with the aim of obtaining a co-amorphous system and determining the potential intermolecular interactions. These systems were fully characterized by differential scanning calorimetry (DSC), FT-infrared spectroscopy (FTIR), X-ray powder diffraction (PXRD), scanning electron microscopy (SEM) and solid state Nuclear Magnetic Resonance (ssNMR). The co-grinding process was not useful to get a co-amorphous system but it led to obtaining the 1:1 CGMa disordered phase. Moreover, in this system both FTIR and ssNMR

analysis strongly suggest intermolecular interactions between the sulfoxide group of omeprazole and the primary amine of amoxicillin anhydrous. The solubility measurements were performed in simulated gastric fluid (SGF) to prove the effect of the co-grinding process. Complementarily, we carried out density functional theory calculations (DFT) followed by quantum theory of atoms in molecules (QTAIM) and natural bond orbital (NBO) analyses in order to shed some light on the principles that guide the possible formation of heterodimers at the molecular level, which are supported by spectroscopic experimental findings.

Keywords: Omeprazole; Amoxicillin; Drugs Interactions; disordered phases; DFT; QTAIM; NBO; FTIR; ssNMR

Introduction

Amoxicillin trihydrate (AMX) belongs to the penicillin class of antibiotics, being a β-lactam antibiotic used to treat bacterial infections caused by susceptible microorganisms. AMX is classified as class III according to the Biopharmaceuticals Classification System (BCS) [1]. Omeprazole (OMZ), a gastric proton-pump inhibitor (H^+/K^+-ATPase), is widely used for the prevention and treatment of stomach and esophagus diseases [2]. Moreover, OMZ is a slightly water-soluble drug and is classified as class II by the BCS. Both, OMZ and AMX are supplied for the treatment of *Helicobacter pylori* eradication [3], which plays an important role in duodenal and gastric ulcer pathologies.

The amorphization of a poorly water-soluble drug can be a useful strategy to enhance its solubility, intrinsic dissolution rate and its bioavailability, which comes as a result of an excess of free energy, compared to that of the crystalline counterpart [4]. However, the amorphous form, being a higher energy state, is physically unstable and leads to the release of excess energy by structural relaxation, going to a lower energy form during storage, which is probably transformed into an unwanted crystalline form. Solid dispersion technology, in which a drug is

included into an amorphous polymer, is the most extensive approach to increase the stability of amorphous systems [5], but this method has shown several disadvantages which were reported by Riikka Laitinen *et al* [6]. An alternative approach is the synthesis of co-amorphous systems, where a combination of two small molecules, either *Active Pharmaceutical Ingredients (API)* - *Generally Recognized As Safe* (GRAS) or API - API, is used instead of drug-polymer mixtures. The improved physical stability and dissolution of these co-amorphous systems is attributed to new intermolecular interactions between the components of the binary system [5,6], which improves physical-chemical properties compared to the pure drugs, particularly solubility and dissolution rate. Several techniques have been used to prepare co-amorphous binary systems: solvent evaporation [7,8], quench cooling [9], grinding [10-12] and so on. The latter could induce defects in the crystal lattice [13,14] altering both the physical and chemical properties of the pharmaceutical ingredients [15,16]. These defects produce disordered phases rather than amorphous compounds and show X-ray patterns similar to both amorphous systems [14,17] and poorly crystalline [18], while the DSC analysis may or may not detect the glass transition temperature (Tg) [14,17,18].

Within the past few decades, quantum mechanical (QM) chemistry has become increasingly used in the pharmaceutical field, especially due to its applicability in the assignment of vibrational spectra [19]. QM calculations have also been employed for the band assignment of the experimental infrared (IR) and Raman spectra of drugs [20-23]. Especially in the case of amorphous materials, QM calculations can become a powerful tool to get further insight in the near range order of amorphous systems and to help interpret and support experimental spectra. The situation becomes more complex in mixed systems such binary systems of APIs, systems for which the QM calculations could provide a clearer insight. In this paper, the binary systems OMZ-AMX, (CGM samples), in addition to OMZ-AMXa, (anhydrous amoxicillin) (CGMa

samples), in 3:7, 1:1 and 7:3 molar ratios, respectively, were obtained by co-grinding with the aim to achieve co-amorphous phases and elucidate the potential intermolecular interactions. Although the daily OMZ-AMX molar ratios indicated for the patients are different from the molar ratios used in this study, the latter were selected to account for spectroscopic, thermal or structural changes expected in the molecular environments might be undetectable or lost and as such might be not observable. The physicochemical properties were investigated with an appropriate combination of different techniques such as powder X-ray diffraction (PXRD), FT-infrared spectroscopy (FTIR), differential scanning calorimetry (DSC) and solid state Nuclear Magnetic Resonance (ssNMR). Assays of solubility were determined by HPLC in simulated gastric fluid (SGF). Moreover, density functional theory (DFT) calculations, Quantum Theory of Atoms in Molecules (QTAIM) and Natural Bond Orbital (NBO) were employed to shed some light on the possible formation of heterodimers according to the modes of interactions proposed by spectroscopic techniques (FTIR and ssRMN) between both APIs.

2. Experimental

2.1. Materials

OMZ (MW: 345.42 g mol^{-1}) was purchased from Sigma-Aldrich® and used without any further purification. AMX (MW: 419.45 g mol^{-1}) was provided by the Drug Quality Control Laboratory (National University of San Luis, San Luis, Argentina). The purity of the samples was checked by thin layer chromatography. In Figure 1 the chemical structures and atom numbering corresponding to OMZ and AMX are shown.

2.2. Methods

2.2.1. OMZ-AMX binary systems preparation (PM and CGM samples)

A total of 1 g of fresh binary mixtures of OMZ and AMX in 7:3, 1:1 and 3:7 molar ratios were mixed with a similar tumbling mixer during 10 minutes and named 7:3, 1:1 and 3:7 physical mixtures (PM), respectively. The PM samples were prepared in triplicate. The samples named co-ground mixture (CGM) in 7:3, 1:1 and 3:7 molar ratios were obtained by manually grinding 500 mg of the PM samples for 60 minutes, in an agate mortar at 25 °C. Moreover, 250 mg of pure OMZ and AMX were ground during 60 minutes and then it was confirmed by FTIR and PXRD that the mechanical treatment did not alter their spectroscopic and structural properties (data not shown). All samples were kept in the dark at 4 ± 2 °C in a desiccator with silica for further examination.

2.2.2. OMZ-AMXa binary systems preparation (PMa and CGMa samples)

A total of 100 mg of physical mixture and co-ground mixtures with amoxicillin anhydrous, (PMa and CGMa samples, respectively), in 7:3, 1:1 and 3:7 molar ratios, were prepared as described in Section 2.2.1 but using AMXa. In order to prevent the rehydration of AMXa during grinding, this process was carried out in a PVC bag at 25 °C with silica gel. Amoxicillin anhydrous was obtained placing AMX in a DSC equipment (see 2.3.1. section) and heating to the dehydration temperature; HPLC analysis shows that the chemical integrity of AMXa is not altered by the dehydration process (Figure S1). The samples were maintained in the dark at 4 ± 2 °C in a desiccator with silica for further examination.

2.2.3. Stability studies

2.2.3.1. Physical stability: The physical stability of the X-ray amorphous samples, AMXa and 1:1 CGMa, kept under dry conditions in a desiccator at 4, 25 and 40 ºC for 45 days, was determined by PXRD and DSC analysis.

2.2.3.2. Chemical stability: The chemical stability of the X-ray amorphous samples, AMXa and 1:1 CGMa, stored for 45 days to 4, 25 and 40 °C was evaluated by HPLC. The analysis

was performed by dissolving a known amount of the sample in 50% (V/V) acetonitrile-DMSO solution and analyzing the sample by HPLC (see section 2.3.5). No additional peaks corresponding to degradation products were observed in the chromatograms (Figure S2), suggesting that the storage condition does not alter the chemical integrity of the samples.

2.2.4. Solubility assays

The solubility studies of OMZ, AMX, AMXa and 1:1 CGMa were carried out in simulated gastric fluid (SGF) free of enzymes [24]. An excess of the samples was added to 10 mL of dissolution medium. These suspensions were shaken in a JEIO TECH SI-300R shaker at 100 rpm for 40 minutes at 37 °C. The resulting suspensions appropriately diluted were filtered with a 0.22 μm Millipore® membrane filter. The concentration of the drugs was chromatographically determined by HPLC (see 2.3.5. section). All data are presented as the mean of three individual observations with the corresponding standard deviation. The method used to quantify both drugs was linear in the range of 0.345-2.487 g L^{-1} for OMZ (R^2: 0.9990) and 0.167-4.194 g L^{-1} for AMX (R^2: 0.9950).

2.3. Analytical techniques

2.3.1. Thermal analysis

DSC curves were obtained with a Shimadzu TA-60WS Thermal Analysis System using 3-4 mg of the powder in open aluminum pans, in flowing air, at 50 mL min^{-1} and with a heating rate of 10 ºC min^{-1} from room temperature to 250 ºC.

Thermogravimetrical Analyses (TGA) were performed using a Shimadzu TGA-51 Thermal Analyzer using platinum pans, flowing air at 50 mL min^{-1} and a heating rate of 10 ºC min^{-1} from RT to 800 ºC.

2.3.2. FT-Infrared spectroscopy (FTIR)

FTIR spectra were recorded on a Nicolet PROTÉGÉ-460 spectrometer provided with a CsI beamsplitter in the 4000-400 cm^{-1} range, with 64 scans and a spectral resolution of 2 cm^{-1}, using the KBr pellet technique. Attenuated total reflectance (ATR) curves were recorded on a FTIR spectrometer model Varian 640-IR. No differences between FTIR and ATR spectra were found for the samples, which allowed us to confirm that the KBr disk technique does not alter the normal IR modes.

2.3.3. X-ray powder diffractometry (PXRD)

XRD diagrams were obtained in a Rigaku D-MAX IIIC diffractometer using Cu K_α radiation (Ni-filter). The diffractograms were recorded in the 2θ angle range of 5-40º, and the process parameters were set at 0.02 2θ scan step size and 2s scan step time.

2.3.4. Solid state Nuclear Magnetic Resonance (ssNMR)

The analysis was carried out through ^{13}C-CPTOSS, 2D-(^{1}Hx^{13}C)-FSLG-HETCOR and ^{15}N-CPMAS experiments. All the experiments were recorded on a Bruker Avance-III-400 spectrometer operating at 400 MHz for ^{1}H, and equipped with a 4.0 mm double resonance MAS probe. The samples were packed in a 4 mm zirconia MAS rotor. In ^{13}CCPTOSS pulse sequence experiments, the Hartmann–Hahn polarization transfer was optimized with a contact time of 2 ms with a 90º pulse length of 5.0 μs, recovering time of 5 s, number of scans equal to 4096, and spinning speed of 5 kHz. For ^{15}N-CPMAS, the contact time used was 3 ms and the number of scans was about 20000 (about 24 h), the recovering time was also 5 s. For (^{1}Hx^{13}C)-FSLG-HETCOR the contact time was 200 μs for all the experiments. The rotor containing the sample was spun at 10 KHz, and the average experiment time was 14 h for each sample.

2.3.5. HPLC determinations

HPLC measurements were performed using a Gilson 322 series pump with a ThermaSphereTS-

130 HPLC temperature controller, a Rheodyne7725i sample injector, and a Gilson 152 UV-vis detector. The analysis was carried out with a Luna C18(2) column (5 μm, 250 mm x 4.6 mm) from Phenomenex. The chromatographic studies were performed with a mobile phase of acetonitrile - phosphate buffer (pH 6.5 ± 0.05; 0.2 M) 70:30 (v/v), respectively. The mobile phase was pumped at a flow rate of 1 mL min^{-1}, and the detector was set at 240 nm.

2.4. Computational methods

The geometries assumed by the heterodimer were characterized at the DFT theory by using two functional: MPW1B95 and B3LYP. While the latter is a popular density functional, the former is of broad application and both give a good performance for hydrogen bond (H-bond) and a weak interaction calculation [25-28]. All calculations were carried out with the Gaussian 09 package [29]. The conformers were fully optimized at the 6-311G(d,p) basis set with no symmetry constraint and characterized by harmonic frequencies analysis as local minima (all frequencies real). In order to characterize the H-bond intermolecular interaction, the QTAIM [30,31] and NBO [32,33] analyses were done with the wave function obtained at the 6-311+G(3df,2p) basis set. According to QTAIM, a bond critical point (BCP) between two atoms is a universal indicator of bonded interactions while the electron density, $\rho(r)$, at the BCP is related to the bond strength. According to a proposed set of criteria by Koch and Popelier [34], the existence of BCP and the topological properties of $\rho(r)$ at the BCP can be used to deeper understand the nature and strength of hydrogen bonds.

At the NBO formalism, the charge transfer (CT) effects from the H-acceptor to the H-donor due to a rearrangement of electron density after the hydrogen bond formation can be identified from the presence of off-diagonal elements in the Fock matrix [35]. While the strength of the interaction due the electron delocalization, $E^{(2)}$, is estimated by the second-order perturbation

theory as:

$$E^{(2)} = \Delta E_{ij} = q_i \frac{F(i,j)^2}{\varepsilon_j - \varepsilon_i}$$

Where q_i is the donor orbital occupancy, ε_i, ε_j are orbital energies (i.e. diagonal elements) and *F(i,j)* is the off-diagonal NBO Fock matrix element.

3. Results and discussion

3.1. Characterization of CGM samples

The DSC profiles corresponding to the pure drugs (OMZ and AMX) are in agreement with the previously reported [36-38]. Furthermore, the DSC curves of the grinding pure drugs (Figure 2B (a) and (e)) show no changes when compared with the not ground pure drugs (Figure 2A (a) and (e)). This indicates that the mechanical process does not modify the thermal properties of OMZ and AMX. The DSC profiles of PM samples (Figure 2A) appear as an overlap of those of the pure drugs, while in CGM samples (Figure 2B) there is a substantial size reduction of the OMZ melting endotherm which could be attributed to a reduction of drug crystallinity [39]. The XRD patterns of the CGM binary systems (Figure 3B) show diffraction peaks in the same position than the PM samples (Figure 3A). However, in the CGM binary systems, a peaks broadening of OMZ and AMX is observed which could be attributed to partial amorphization induced by the grinding treatment, which is in keeping with the previous DSC analysis.

The study of intermolecular interactions in CGM samples was performed by FTIR spectroscopy. The FTIR spectra of CGM when compared to PM samples do not show band shifts that could be associated with intermolecular interactions between the two drugs (Figure S3).

3.2. Characterization of the amoxicillin anhydrous (AMXa)

The dehydration process is one of the most important reactions in the solid state due to its potential conversion to a metastable or amorphous phase with an important stability reduction [40]. Before understanding the effect of the AMX dehydration on the CGMa samples, it was necessary to characterize the AMXa in the solid state. The crystal structure of AMX [41] shows that the water molecules are H-bonded to functional groups which could potentially participate in drug-drug intermolecular interactions. Thus, the dehydration leads to a more reactive AMX.

The PXRD pattern showed a characteristic halo of amorphous compounds after AMX dehydration (Figure 4A (a)). However, the typical Tg of amorphous phases was not found by DSC analysis. This fact could be due to some type of disordered phase other than amorphous [14,17]. However, PXRD showed that AMXa remained stable at all tested temperatures over the course of 45 days (data not shown) and no absorption of moisture was observed by DSC analysis during the test period (Figure S4).

Major changes associated with the loss of the crystallization water were observed in the FTIR spectrum of AMXa in comparison with AMX (Figure S5, Table S1). The vibrational modes $\upsilon(C_5=O_1)$, $\upsilon(C_9=O_4)$ and $\upsilon(N_3\text{-}H)$ shift to lower frequencies, while the $\delta(O_5\text{-}H)$ band assigned to the phenolic ring appears at a higher one. The shifting could be associated with the formation of intermolecular interactions present in AMXa.

3.3. Characterization of CGMa samples

Figure 4 compares the XRD patterns of CGMa to the PMa samples. The corresponding PMa diffractograms (Figure 4A) show only the diffraction peaks of OMZ, with the peaks of the AMXa being absent due to its poorly crystalline nature. In the CGMa diffractograms (Figure 4B), the peaks of OMZ are only observed in the 7:3 CGMa (Figure 4B (c)), while a characteristic halo of an amorphous compound is observed in 3:7 and 1:1 CGMa ones (Figure 4B (a) and (b), respectively). The presence of OMZ diffraction peaks in 7:3 CGMa and their

absence in 3:7 CGMa, are due to an excess of OMZ and AMXa, respectively. This is also evident in FTIR analysis, as detailed below. The absence of diffractions corresponding to OMZ in 1:1 CGMa might be due to interactions between both drugs, which destabilize the crystalline structure of OMZ, converting it into a X-ray amorphous phase.

Due to the complexity of the spectra (Figure S5), the FTIR analysis was performed on the basis of the most important functional groups of both drugs. The FTIR spectrum of 3:7 CGMa does not show any AMXa vibrational modes differences with respect to the pure AMXa ones, while in the corresponding 7:3 CGMa spectrum, no band shifts were observed for OMZ when compared to pure OMZ. These findings indicate an excess of AMXa and OMZ in 3:7 and 7:3 CGMa, respectively. Consequently, the FTIR spectrum of 1:1 CGMa sample was analyzed.

The vibrational behavior of 1:1 CGMa sample clearly shows evidence of drug-drug interactions (Figure 5, Table S1). The major band shifts are observed for $\upsilon(N_3\text{-}H)$ and $\delta(N_3\text{-}H)$ of the primary amine of AMXa and the $\upsilon(S_1{=}O_2)$ of OMZ (Table S1). Moreover, slight band shifts are observed for $\delta(O_5\text{-}H)$, $\upsilon(C_9\text{-}N_2)$ and $\upsilon(C_5{=}O_1)$ in AMXa and $\upsilon(C_{11}\text{-}O_3\text{-}C_{16})$, $\upsilon(C_5\text{-}O_1\text{-}C_{17})$ and $\upsilon(C_1{=}N_2)$ in OMZ.

Taking into account that the 3:7 and 7:3 CGMa samples show excess of AMXa and OMZ respectively, the 1:1 CGMa binary system was analyzed by ssNMR of ^{13}C, ^{15}N and 2D-heteronuclear experiments (Figure S6) to evaluate the interaction previously proposed by FTIR spectroscopy. No changes in the ^{13}C chemical shifts of AMXa and OMZ in the 1:1 CGMa binary system were observed when comparing the spectra of the isolated molecules; however, a weak interaction between the drugs molecules could not be discarded. After the analysis of ^{15}N ssNMR spectra, the chemical shifts were evaluated in order to assess a possible H-bond formation. The signal corresponding to N_3 of AMXa shows an increasing chemical shift from

19.04 to 23.80 ppm which might corroborate the interaction previously proposed by FTIR analysis in this sample. A small chemical shift in the ^{15}N spectra has been previously observed where primary amine participates in H-bonds interactions [42,43]

It is found in the literature that ^{1}H ssNMR is the best probe to detect hydrogen bonds [44]. However, the acquisition of hydrogen spectrum in solid state NMR is not trivial, since its intense dipolar coupling yields very broad lines. Over the last 10 years many techniques have been developed to circumvent this problem. One of these techniques proposes the acquisition of a FSLG-HETCOR ($^{1}Hx^{13}C$) experiment in order to minimize the ^{1}H-^{1}H dipolar interaction, thus obtaining a better resolved ^{1}H ssNMR spectrum, which can be extracted from the hydrogen projection. A rough comparison between the ^{1}H ssNMR projection obtained from 2D-heteronuclear experiments of isolated molecules and the 1:1 CGMa sample provides us with information about the interaction between both drugs, since the N_3H signal of AMXa (about 12 ppm) completely disappears.

Figure 6 shows the thermal behavior of the 1:1 CGMa. An endothermal signal is observed at 25.1 °C, without associated changes in the TGA curve. Despite this single signal could be associated to the Tg (considering the lack of diffraction peaks showed in Figure 4B (b)) its form does not fit the typical Tg. Taking these facts into account, the thermal event could be associated to solid state re-arrangement. The physical stability is not altered as will be discussed below.

Physical stability of 1:1 CGMa was analyzed by PXRD and DSC (Figure S7). No diffraction peaks were observed indicating that the sample maintains its amorphous nature at all tested temperatures. The DSC curves of 1:1 CGMa stored at 4, 25 and 40 °C show neither crystallization exotherms nor melting endotherms, serving as an additional evidence to the fact that the system is physically stable.

Considering the described behavior, 1:1 CGMa could be classified as a disordered phase (it is X-ray amorphous and does not show Tg) [14,17].

4. DFT calculations

Since the experimental evidences indicate the intermolecular interactions in 1:1 CGMa, heterodimers composed by OMZ and AMXa are defined for the DFT study. Three conformers for the OMZ-AMXa heterodimer were proposed to take into account the FTIR (Figure 5) and the ssNMR results. These conformers were fully optimized by using the B3LYP and MPW1B95 functional and a uniform 6-311G(d,p) basis set. As shown from Table S2, the conformer 3 has the lowest energy at both functionals. The experimental and DFT vibrational modes are listed in Table S1. The DFT calculations correspond closely with the experimental data, although the MPW1B95 functional was the most suitable method to describe the experimental FTIR. The spectral $\Delta_{|DFT - experimental|}$ fell into the ranges of 174 - 9 cm^{-1} and 67 - 0.05 cm^{-1} by the B3LYP and MPW1B95 functionals, respectively. According to the previous results, the conformers obtained by geometry optimization at the MPW1B95 functional (Figure 7) were taken to perform the QTAIM and NBO analysis.

4.1. QTAIM analysis: One way to study the nature and strength of the H-bond interactions is to analyze the topological properties of the *ab initio* wave function by using Bader's theory [45,46]. Briefly, the quantum theory of atoms in molecules (QTAIM) allows us to partition a molecule wave function into atomic basins and, thus, to indentify and characterize the strength of the H-bond interactions between atoms trough an analysis of the local properties at the bonding critical points (BCPs). In this work, the charge density (ρ) and its Laplacian ($\nabla^2\rho$) were the topological properties analyzed. The molecular graphs of the proposed conformer, the

BCP and bond path are shown in Figure 7, while their topological properties are listed in Table 1.

Koch and Popelier proposed a set of criteria based in the QTAIM theory to evaluate the hydrogen bonding [34]. The presence of a BCP between the hydrogen and the acceptor atom, and a bond path connecting these two atoms are found in all H-bonds interactions (Figure 7). The analyses of the charge density and its Laplacian have been recommended to determine the strength corresponding to H-bonds interactions. As can be seen in Table 1, the ρ and $\nabla^2\rho$ values corresponding to all C-H···O/N H-bonds intermolecular interactions (non classical H-bonds interactions) fall in the range proposed by Koch and Popelier (ρ: 0.002-0.034 a.u. and $\nabla^2\rho$: 0.024-0.139 a.u.) [34]. For N_3-H···O_2 H-bond intermolecular interactions the $\nabla^2\rho$ values are within the proposed range, while the ρ values exceed the upper limit. These findings might be indicative of a strong interaction between OMZ and AMXa, being in the conformer III the strongest interaction due to higher values of ρ [47].

Moreover, the electronic energy density, K(r), can also be indicative of the strength of the H-bond [48]. For strong H-bond, K(r) adopts positive values, whereas negative values suggest weak hydrogen bonds. In keeping with the previous assumption, conformer III shows two strong H-bond interactions (partially covalent and partially electrostatic) while conformers I and II show only one. Those corresponding to the latter have a higher K(r) value, therefore corroborating the relative stability previously calculated (Table S2).

4.2. NBO analysis: The delocalization energy $E^{(2)}$ values associated with the intermolecular H-bond between OMZ and AMXa are listed in Table 2. The second-order theory analysis of the Fock matrix shows that the N_3-H···O_2 intermolecular H-bond is the strongest of the three conformers. All interactions are formed between the nitrogen, sulfur or oxygen lone pairs (n_B)

with the antibonding orbital (σ^*_{XH}) corresponding to the hydrogen atom in the X-H moiety. The largest $E^{(2)}$ value is found in conformer III, followed by conformer II and, finally, conformer I.

5. Solubility assays

The solubility assays was carried out in SGF as indicated in the experimental section. Under these conditions, (pH: 2 and 37 °C), OMZ and AMX are unstable [48,49]; however, in this work, the solubility parameters were evaluated at 40 minutes, so the degradation products are kept minimum. The solubility values of the pure drugs, OMZ (0.31 ± 0.03 g L^{-1}), AMX (4.74 ± 0.60 g L^{-1}) and AMXa (6.25 ± 0.37 g L^{-1}) in comparison with the 1:1 CGMa binary system (AMXa: 8.44 ± 0.31 g L^{-1} and OMZ: 0.36 ± 0.03 g L^{-1}) evidenced that the co-grinding process causes an improvement in the solubility values of both drugs, this fact being probably due to new intermolecular interactions between them. Moreover, the increased solubility agrees with the previously described X-ray amorphous nature.

Conclusions

The CGM and CGMa binary systems were obtained by co-grinding with the aim of achieving co-amorphous phases and elucidating the potential intermolecular interactions. In the CGM samples, a decrease in the crystallinity of the parental drugs is observed by DSC and PXRD analysis. The study of the interactions at the molecular level does not show band shifts that could be associated with intermolecular interactions between the two drugs.

In 1:1 CGMa samples, a characteristic halo of amorphous compound was observed by PXRD and an endotherma shown in DSC curve associated to solid-solid re-arrangement allow us to describe this binary system as a disordered phase, rather than a co-amorphous one. Its vibrational behavior shows evidence of OMZ-AMXa intermolecular interactions through the

sulfoxide group of the OMZ and the primary amine of the AMX. This interaction proposed by FTIR analysis might be corroborated through an increasing chemical shift in the N_3 signal of AMXa observed in the ^{15}N ssNMR spectrum and the complete disappearance of the N_3H signal of AMXa in the ^{1}H ssNMR projection obtained from 2D-heteronuclear experiments. The solubility measurements of 1:1 CGMa indicate that the co-grinding process improves this property in relation to the pure drugs.

The DFT calculations, using the MPW1B95 functional, show good agreement with the experimental FTIR data. The ρ and $\nabla^2\rho$ values corresponding to all C-H···O/N H-bonds intermolecular interactions are in between accepted values; however, the ρ values of N_3-H···O_2 H-bond exceed the upper limit. These findings might be indicative of a strong interaction between OMZ and AMXa, with the strongest interaction being in conformer III due to higher ρ values. Concordantly, the NBO analysis indicate that conformer III shows the largest $E^{(2)}$ value providing evidence that a strong N_3-H···O_2 intermolecular H-bond is formed by the interaction of the oxygen lone pair with the H-N antibonding orbital. The QM calculations in combination with FTIR spectroscopy prove to be a powerful tool in interpreting the molecular near range order of a co-amorphous sample.

Aknowledgments

This work was supported by the PIP CONICET 112-201101-00912; ANPCyT PICT-2012-1994 and Universidad Nacional de San Luis (PROICO 2-1612); T. V. thanks FAPESP (Project 2009/13860-2). J. E. thanks CNPQ and FAPESP for financial support. M.G.R. thanks the CONICET fellowship. G.E.N. and H.A.Baldoni are members of CIC-CONICET.

References

[1] Y. Tsume, G.L. Amidon, Mol. Pharmaceutics 7 (2010) 1235-1243.

[2] D.Y. Lee, H.S. Shin, S.K. Bae, M.G. Lee, Biopharm. Drug. Dispos. 27 (2006) 209-218.

[3] J.C. Yang, H.L. Wang, H.D. Chern, C.T. Shun, B.R. Lin, C.J. Lin, T.H. Wang, Pharmacotherapy 3 (2011) 227-238.

[4] B.C. Hancock, M. Parks, Pharmaceut. Res. 17 (2000) 397-404.

[5] N. Chieng, T. Rades, J. Aaltonen, J. Pharm. Biomed. Anal. 55 (2011) 618 – 644.

[6] R. Laitinen, K. Lobmann, C. J. Strachan, H. Grohganz,T. Rades, Int. J. Pharm. 453 (2013), 65–79.

[7] S.J. Dengale, S.S. Huseen, B.S.M. Krishna, P.B. Musmade, G.G. Shenoy, K. Bhat, Eur. J. Pharm. Biopharm. 83 (2015), 329-338.

[8] S.J. Dengale, O.P. Ranjan. S.S. Hussen, B.S.M. Krishna, P.B. Musmade, G.G. Shenoy, K. Bhat, Eur. J. Pharm. Biopharm. 62 (2014), 57-64.

[9] K. Löbmann, R. Laitinen, H. Grohganz, C. Strachan, T. Rades, K.C. Gordon, Int. J. Pharm. 1 (2013), 80-87.

[10] M. Alleso, N. Chieng, S. Rehder, J. Rantanen, T. Rades, J. Aaltonen, J. Contolled Release 136 (2009), 45-53.

[11] Chieng, N., Aaltonen, J., Saville, D., Rades, T., Eur. J. Pharm. Biopharm. 71 (2009), 47-54.

[12] Lobmann, K., Grohganz, H., Laitinen, R., Strachan, C., Rades, T., Eur. J. P harm. Biopharm. 85 (2013), 873-871.

[13] S. Bates, R.C. Kelly, I. Ivanisevic, P. Schields, G. Zografi, A.W. Newman, J. Pharm. Sci. 96 (2007) 1418-1433.

[14] T. Feng, R. Pinal, M.T. Carvajal, J. Pharm. Sci. 97 (2007) 3207-3221

[15] R. Huttenrauch, S. Fricke, P. Zielke, Pharm. Res. 6 (1985) 302-306.

[16] E. Shalaev, M. Shalaeva, G. Zogrofi, J. Pharm. Sci. 91 (2002) 584-593.

[17] T. Feng, S. Bates, M.T. Carvajal, Int. J. Pharm. 367 (2009) 16-19.

[18] P. Chakravarty, S. Bates, L. Thomas, Mol. Pharm. 10 (2013) 2809-2822

[19] K.C. Gordon, C.M. McGoverin, C.J. Strachan, T. Rades, J. Pharm. Pharmacol. 59 (2007) 271–277

[20] H.R.H. Ali, H.G.M. Edwards, J. Kendrick, T. Munshi, J.J. Scowen, J. Raman Spectrosc. 38 (2007) 903–908.

[21] A. Borba, A. Gomez-Zavaglia, R. Fausto, J Phys. Chem. A 113 (2009) 9220–9230.

[22] Y. Hu, A. Erxleben, A.G. Ryder, P. McArdle, J. Pharm. Biomed. Anal. 53 (2010) 412–420

[23] A. Srivastava, S. Mishra, P. Tandon, S. Patel, A.P. Ayala, A.K. Bansal, H.W. Siesler, J. Mol. Struct. 964 (2010) 88–96.

[24] J.J. Passos, F.B. De Sousa, I.S. Lula, E.A. Barreto, J.F. Lopes, W.B. De Almeida, R.D. Sinisterra, Int. J. Pharm. 444 (2013) 201-212.

[25] Y. Zaho, D.G. Truhlar, J Phys. Chem. A 33 (2004) 6908-6918.

[26] T.Y. Lai, C.Y. Yang, H.J. Lin, C.Y. Yang, W.P. Hu, J. Chem. Phys. 134 (2011) 244110-244118

[27] Y. Zhao, O. Tishchenko, D.G. Truhlar, J. Chem. Phys. B 109 (2005) 19046-19051

[28] Y. Zhao, D.G. Truhlar J Phys. Chem. A 109 (2005) 5656–5667.

[29] Gaussian 09, Revision D.01, M. J. Frisch, G. W. Trucks, H. B. Schlegel, G. E. Scuseria, M. A. Robb, J. R. Cheeseman, G. Scalmani, V. Barone, B. Mennucci, G. A. Petersson, H. Nakatsuji, M. Caricato, X. Li, H. P. Hratchian, A. F. Izmaylov, J. Bloino, G. Zheng, J. L. Sonnenberg, M. Hada, M. Ehara, K. Toyota, R. Fukuda, J. Hasegawa, M. Ishida, T. Nakajima, Y. Honda, O. Kitao, H. Nakai, T. Vreven, J. A. Montgomery, Jr., J. E. Peralta, F. Ogliaro, M. Bearpark, J. J. Heyd, E. Brothers, K. N. Kudin, V. N. Staroverov, T. Keith, R. Kobayashi, J. Normand, K. Raghavachari, A. Rendell, J. C. Burant, S. S. Iyengar, J. Tomasi, M. Cossi, N. Rega, J. M. Millam, M. Klene, J. E. Knox, J. B. Cross, V. Bakken, C. Adamo, J. Jaramillo, R. Gomperts, R. E. Stratmann, O. Yazyev, A. J. Austin, R. Cammi, C. Pomelli, J. W. Ochterski,

R. L. Martin, K. Morokuma, V. G. Zakrzewski, G. A. Voth, P. Salvador, J. J. Dannenberg, S. Dapprich, A. D. Daniels, O. Farkas, J. B. Foresman, J. V. Ortiz, J. Cioslowski, and D. J. Fox, Gaussian, Inc., Wallingford CT, 2013.

[30] R.F.W. Bader, Atoms in Molecules: a Quantum Theory; Clarendon Press: Oxford, 1990.

[31] R.F.W. Bader, Chem. Rev. 91 (1991) 893-928.

[32] J.P. Foster, F. Weinhold, J. Am. Chem. Soc., 102 (1980) 7211-7218.

[33] A.E. Reed, L.A. Curtiss, F. Weinhold, Chem. Rev., 88 (1988) 899-926.

[34] U. Koch, P.L.A. Popelier, J. Phys. Chem. 99 (1995) 9747–9754.

[35] A.E. Reed, L.A. Curtiss, F. Weinhold, Chem. Rev. 88 (1988) 899–926.

[36] J. Nugrahani, S. Asyarie, S.N. Soewandhi, S. Ibrahim, Int. J. Pharmacol. 3 (2007) 475-481.

[37] M.A. Ruiz, I. Reyes, A. Parera, V. Gallardo, J. Therm Anal Cal. 51 (1998) 29-35.

[38] Gallico, D.A.,. Guerra R.B, Legendre, A.O., Schnitzler E., Mendes, R.A., Bannach, G., Braz. J. Therm. Anal. (2013) 2, 45 – 49.

[39] A. Figueiras, R.A. Carvalho, L. Ribeiro, J.J. Torres-Labandeira, F.J.B. Veiga, Eur. J. Pharm. Biopoharm 67 (2007) 531-539.

[40] L.Yu, Adv. Drug Deliver Rev. 48 (2001) 27-42.

[41] M.O. Boles, R.J. Girven, P.A.C. Gane, Acta Cryst. B34 (1978) 461-466.

[42] A.T. Vasconcelos, C.C. da Silva, L.H.Q. Queiroz Júnior, M.J. Santana, V. Sousa-Ferreira, F.T. Martins, Cryst. Growth Des. 14 (2014) 4691-4702.

[43] R. Koike, K. Higashi, N. Liu, W. Limwikrant, K. Yamamoto, K. Moribe, Cryst Growth Des 19 (2014) 4510-4518.

[44] F.G. Vogt, J.S. Clawson, M. Strohmeier, A.J. Edwards, T.N. Pham, T.N. WatsonCryst. Growth Des. 9 (2009) 921–937.

[45] R.F.W. Bader, 1990. Atoms in molecules. A quantum theory. New York: Oxford University Press.

[46] R.F.W. Bader, Chem. Rev. 91 (1991) 893-928.

[47] J. Zaho, A. Khalizov, R. Zhang, J. Phys. Chem. 113 (2009) 680-689.

[48] P.O. Erah, A.F. Goddard, D.A. Barret, P.N. Shaw, R.C. Spiller, J. Antimicrob. Chemoth. 39 (1997) 5-12.

[49] M. El-Badry, E.J. Taha, F.K. Alanazi, I.A. Alsarra, J. Drug Del. Sci. Tech. 19 (2009) 347-351.

Figure Captions

Figure 1: Chemical structure and numbering of selected atoms of AMX (A) and OMZ (B).

Figure 2: DSC curves of ground and not-ground pure drugs, PM and CGM samples. A: AMX (a); PM 3:7 (b), 1:1 (c) and 7:3 (d); OMZ (e). B: ground AMX (a); CGM 3:7 (b), 1:1 (c) and 7:3 (d); ground OMZ (e).

Figure 3: Diffractograms of ground and not-ground pure drugs, PM and CGM samples. A: AMX (a); PM 3:7 (b), 1:1 (c) and 7:3 (d); OMZ (e). B: ground AMX (a); CGM 3:7 (b), 1:1 (c) and 7:3 (d); ground OMZ (e).

Figure 4: Diffractograms of PMa, CGMa and AMXa. A: AMXa (a); PMa 3:7 (b), 1:1 (c) and 7:3 (d); OMZ (e). B: CGMa 3:7 (a), 1:1 (b) and 7:3 (c); ground OMZ (e).

Figure 5: FTIR spectra of OMZ (a), 1:1 CGMa (b) and AMXa (c). The vibrational modes of OMZ are denoted in red while the corresponding to AMXa in black.

Figure 6: Thermal behavior of 1:1 CGMa. DSC (red) and TGA (black) curves.

Figure 7: Molecular graphs for conformers 1 (A), 2 (B) and 3 (C) optimized at the MPW1B95 functional. The BCP (green dots) between OMZ and AMXa are shown.

Table 1: Geometrical and topological parameters corresponding to H-bonds involved in intermolecular interactions.

	D-H···A(Å)	D-H (Å)	D···A (Å)	H···A (Å)	D-H···A (°)	ρ	$\nabla^2\rho$	K(r)
Conformer I	C_{17}-H···O_3	1.098	3.229	2.411	136.623	0.011075	0.035626	-0.001237
	C_6-H···O_3	1.092	3.222	2.292	155.982	0.018111	0.070554	-0.002622
	N_2-H···S_1	1.023	3.565	2.570	152.776	0.013110	0.032718	-0.000835
	N_3-H···O_2	1.082	2.610	1.590	154.745	0.059852	0.136879	0.011086
	C_8-H···O_4	1.096	3.302	2.263	157.256	0.013574	0.046448	-0.001716
	C_{10}-H···N_4	1.097	3.436	2.553	136.699	0.010223	0.028591	-0.001128
Conformer II	N_3-H···O_2	1.113	2.572	1.578	165.858	0.081406	0.126162	0.025929
	N_2-H···O_1	1.034	2.814	1.801	165.253	0.033307	0.111579	-0.000128
	C_7-H(A)···O_2	1.100	3.691	2.730	145.511	0.005646	0.017346	-0.000664
	C_8-H···O_1	1.100	3.263	2.295	162.896	0.015978	0.053459	-0.001674
	C_{15}-H···O_3	1.100	3.290	2.214	165.418	0.011829	0.033317	-0.000785
	C_{16}-H···O_3	1.105	3.479	2.397	165.778	0.015278	0.051050	-0.001627
Conformer III	N_3-H···O_2	1.127	2.550	1.539	166.873	0.081541	0.133240	0.025599
	N_2-H···O_1	1.044	3.155	2.448	124.125	0.009486	0.033382	-0.001281
	N_2-H···O_3	1.044	2.731	1.850	139.773	0.032768	0.102731	0.000024
	C_6-H···O_3	1.088	3.284	2.336	124.390	0.012661	0.043839	-0.001448
	C_{17}-H···O_2	1.100	3.695	2.707	149.141	0.006430	0.019057	-0.000671

D: Donor. **A**: Acceptor.

ρ: Charge densities; $\nabla^2\rho$: Laplacian; K(r): Total energy densities

Table 2: Second-order perturbation theory results for the H-bond interactions found by the NBO analysis.

	Donor (n_B)	Acceptor (σ^*_{XH})	$E^{(2)}$ (Kcal mol^{-1})	$E_{(j)} - E_{(i)}$ (a.u.)	$F_{(i,j)}$ (a.u.)
Conformer I	O_3	C_{17}-H	0.51	0.53	0.16
	O_3	C_6-H	3.67	0.99	0.054
	S_1	N_2-H	1.88	0.93	0.037
	O_2	N_3-H	18.83	0.53	0.091
	O_4	C_8-H	1.31	0.59	0.026
	N_3	C_{10}-H	0.94	0.64	0.022
Conformer II	O_2	N_3-H	13.97	0.91	0.103
	O_1	N_2-H	9.41	0.98	0.086
	O_2	C_7-H(A)	0.29	1.04	0.016
	O_1	C_8-H	1.51	0.58	0.028
	O_3	C_{15}-H	0.48	0.52	0.016
	O_3	C_{16}-H	1.72	0.93	0.036
Conformer III	O_2	N_3-H	42.33	0.55	0.139
	O_1	N_2-H	1.06	0.57	0.023
	O_3	N_2-H	5.16	0.52	0.051
	O_3	C_6-H	0.47	0.58	0.015
	O_2	C_{17}-H	0.24	0.92	0.013

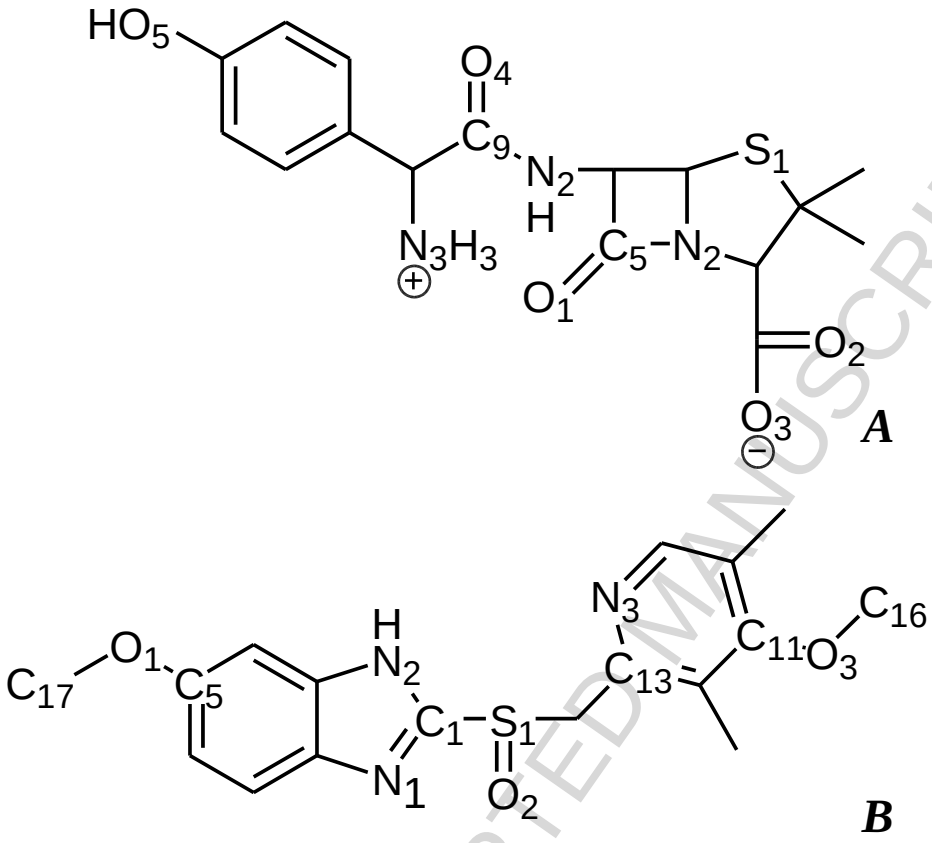

Fig. 1

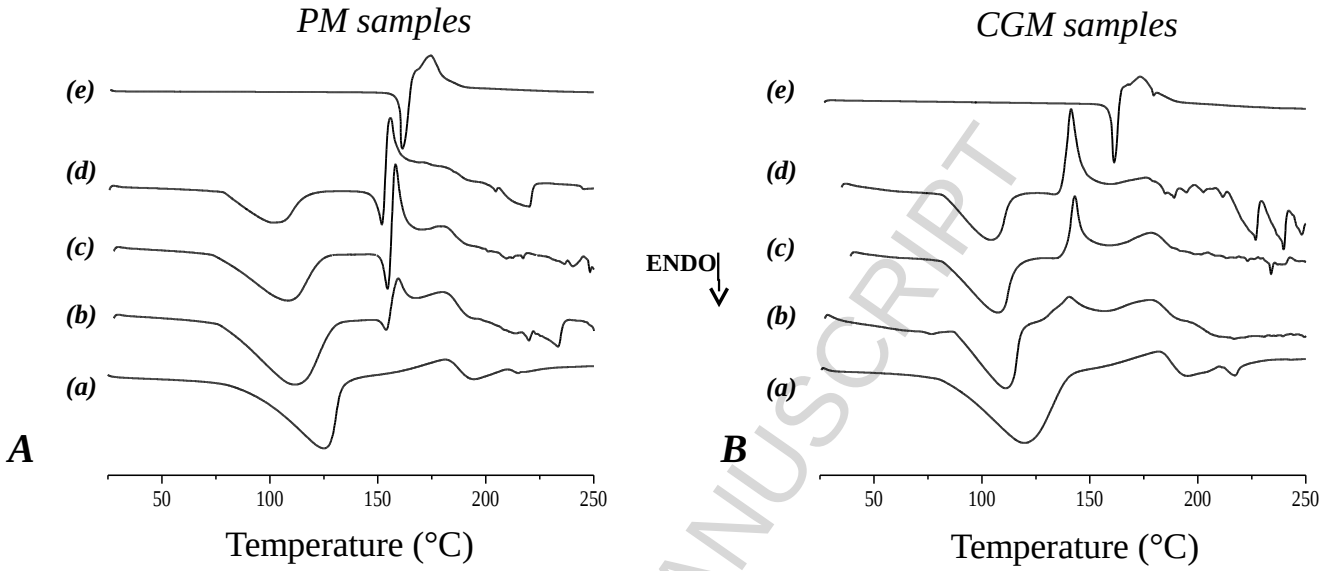

Fig. 2

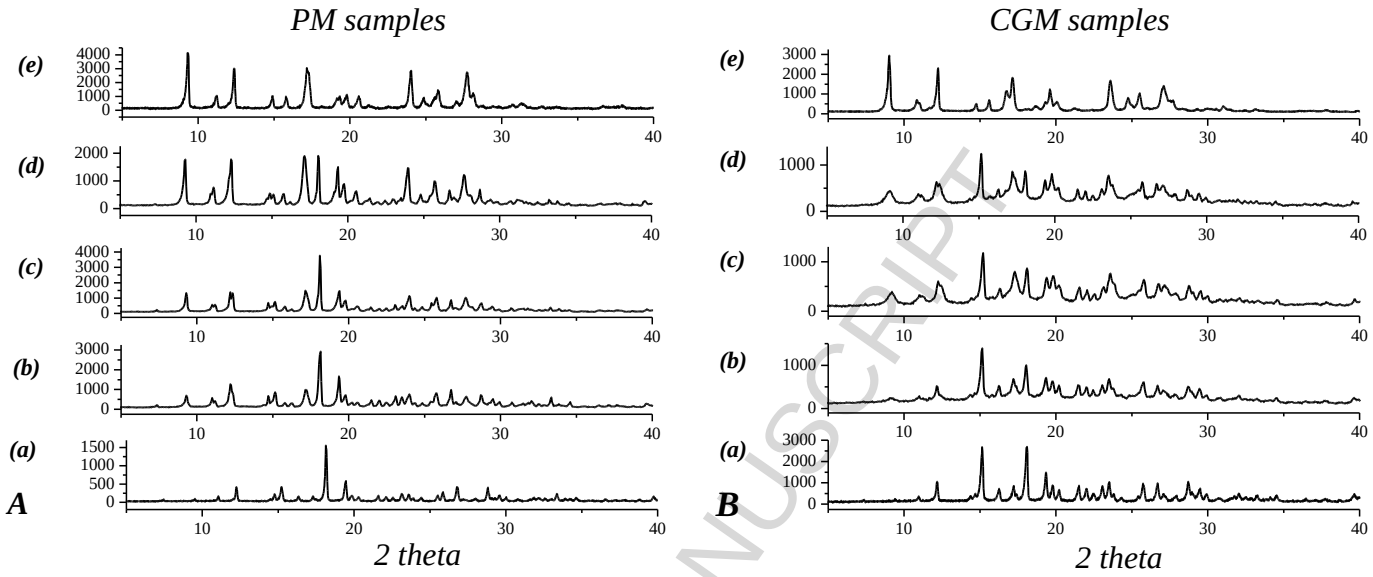

Fig. 3

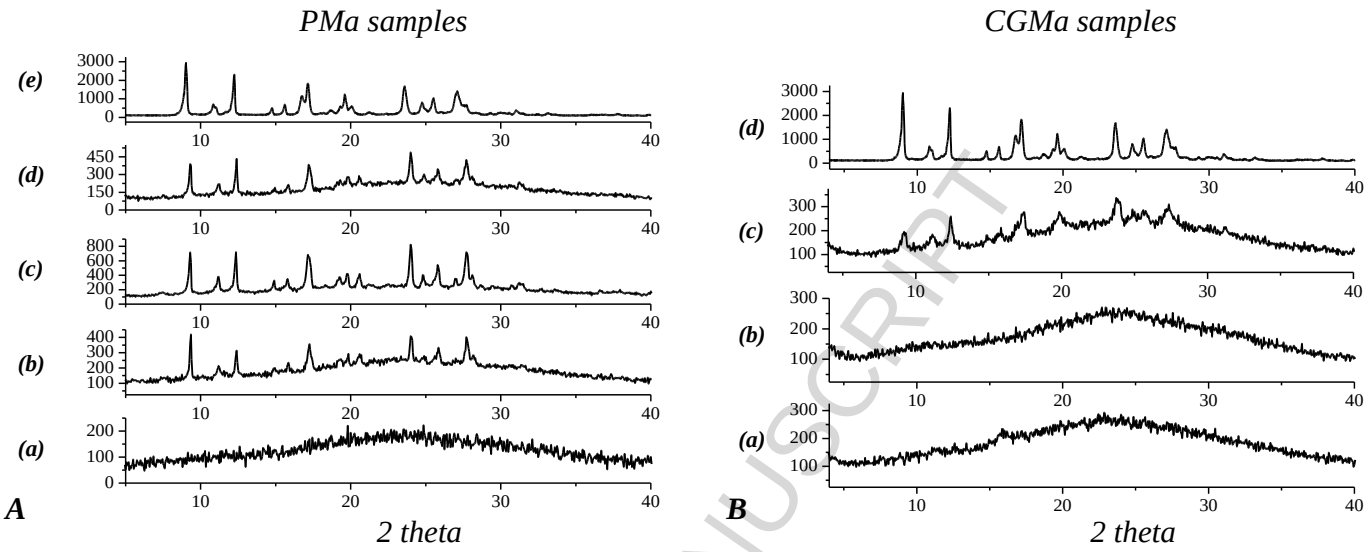

Fig. 4

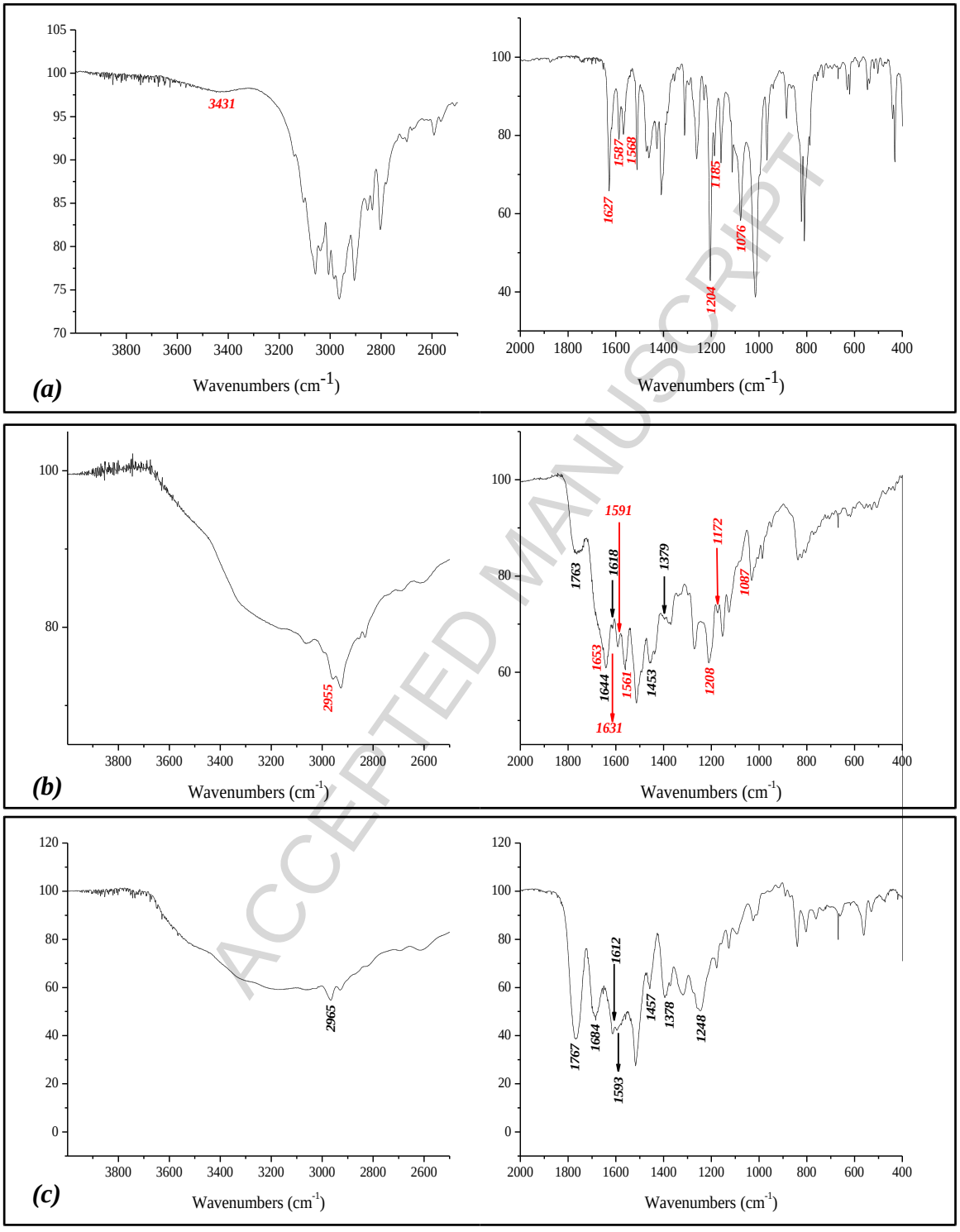

Fig. 5

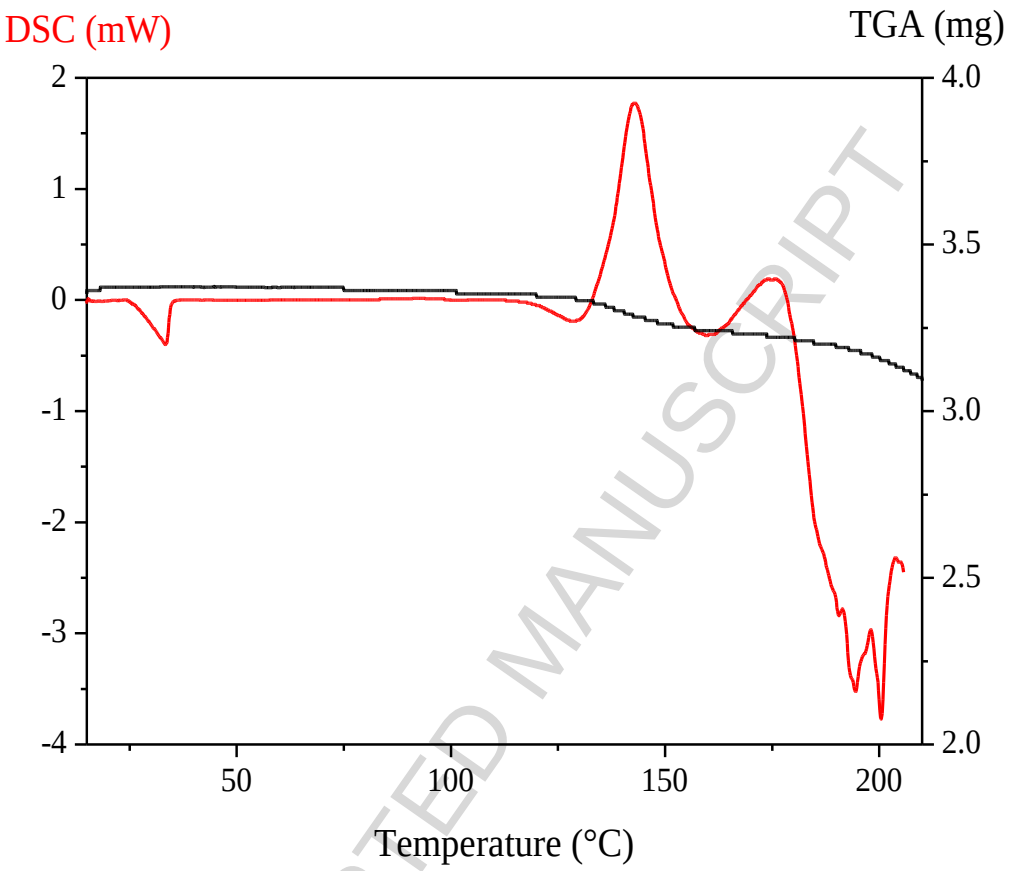

Fig.6

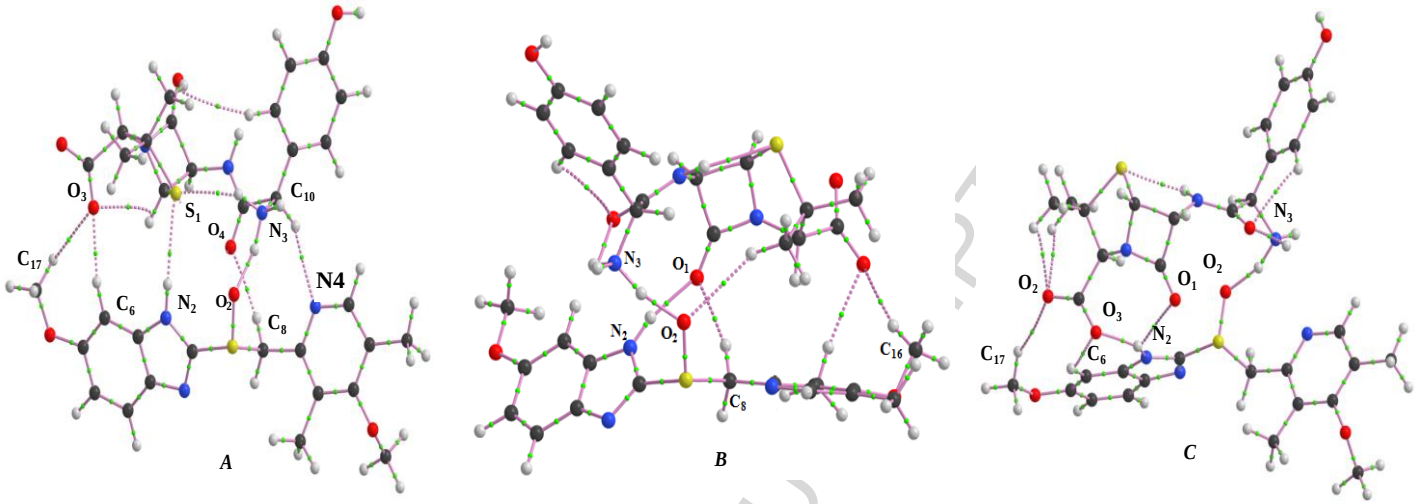

Fig. 7

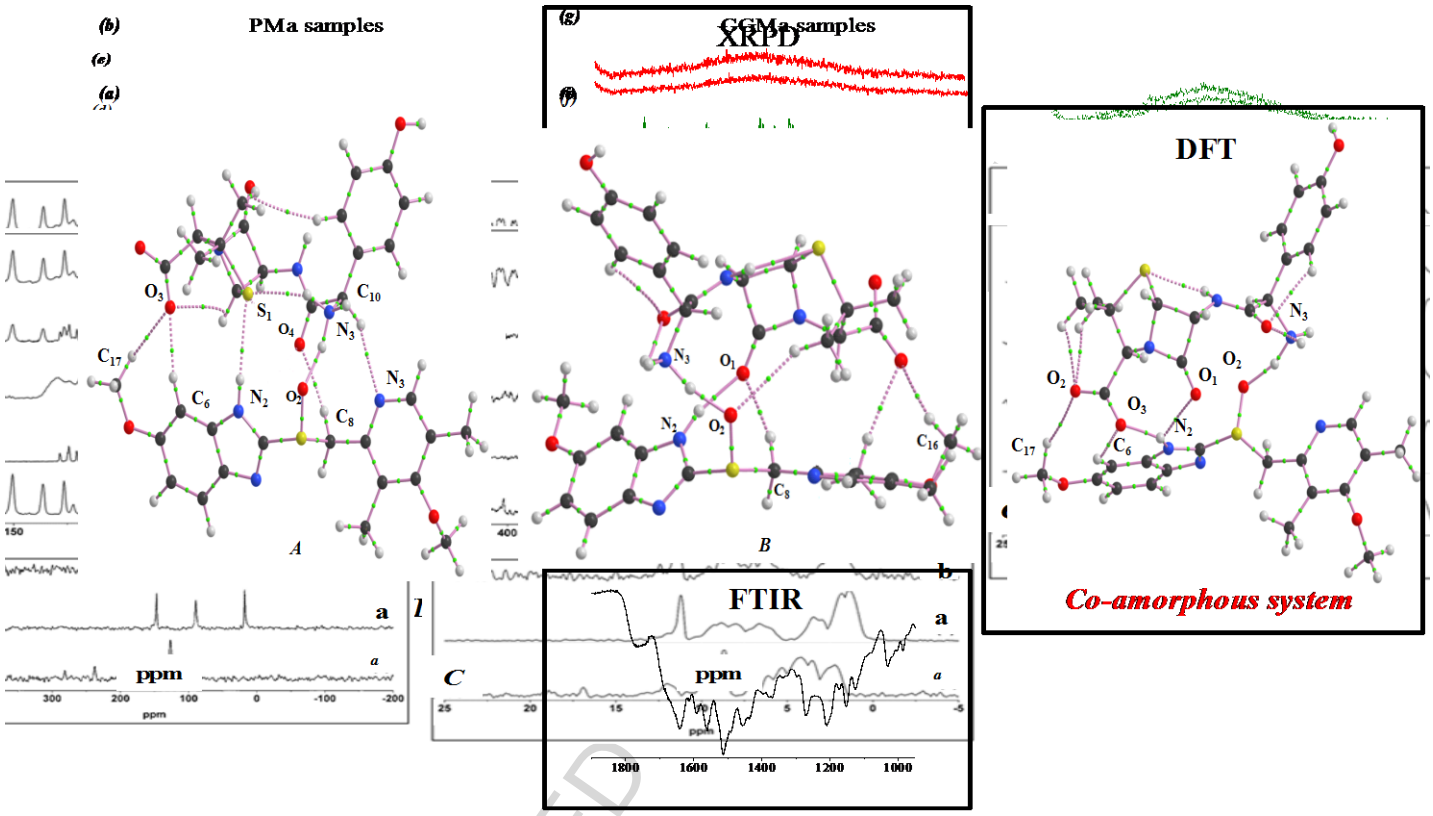

Graphical abstract

Highlights

Omeprazole and anhydrous amoxicillin were obtaining as disordered phase

FTIR and ssNMR spectroscopy strongly suggest intermolecular interactions

B3LYP and MPW1B95 functional were employed to optimized the proposed heterodimers

QTAIM and NBO analyses were performed to analyze the intermolecular interactions